MR. TOMP : INVERSION OF THE MODULO RADON TRANSFORM (MRT) VIA ORTHOGONAL MATCHING PURSUIT (OMP)

Matthias Beckmann[†,‡] *and Ayush Bhandari*[‡]

[†]Center for Industrial Mathematics, University of Bremen, 28359 Bremen, Germany.
[‡]Dept. of Electrical and Electronic Engineering, Imperial College London, SW72AZ, UK.

Emails: research@mbeckmann.de • a.bhandari@imperial.ac.uk

ABSTRACT

In the recent years, practitioners in the area of tomography have proposed high dynamic range (HDR) solutions that are inspired by the multi-exposure fusion strategy in computational photography. To this end, multiple Radon Transform projections are acquired at different exposures that are algorithmically fused to facilitate HDR reconstruction. A single-shot alternative to multi-exposure fusion approach has been proposed in our recent line of work which is based on the Modulo Radon Transform (MRT). In this case, Radon Transform projections are folded via modulo non-linearity. This folding allows HDR values to be mapped into the dynamic range of the sensor and, thus, avoids saturation or clipping. The folded measurements are then mapped back to their ambient range using algorithms. The main goal of this paper is to introduce a novel, Fourier domain recovery method, namely, the OMP-FBP method, which is based on the Orthogonal Matching Pursuit (OMP) algorithm and Filtered Back Projection (FBP) formula. The proposed OMP-FBP method offers several advantages; it is agnostic to the modulo threshold or the number of folds, can handle much lower sampling rates than previous approaches and is empirically stable to noise and outliers. Computer simulations as well as hardware experiments in the paper validate the effectivity of the OMP-FBP recovery method.

Index Terms— Computational imaging, computer tomography, high dynamic range, Radon transform and sampling theory.

1. INTRODUCTION

The *Modulo Radon Transform* (MRT) [1, 2] was recently introduced to enable a single-shot, high dynamic range (HDR) reconstruction approach in the context of Radon Transform measurements. When conventional Radon projections exceed the dynamic range of the detector, the resulting measurements are saturated or clipped, leading to a permanent loss of information. To overcome this bottleneck, in the recent years, independent groups of researchers have explored the idea of HDR tomography [3–6] which is largely inspired by the *multi-exposure fusion* approach in computational photography [7, 8]. By fusing X-ray exposures, for example, at different tube voltages [3], HDR reconstruction has been experimentally verified.

Instead of fusing multiple exposures, we have been exploring an alternative approach based on the MRT [1, 2, 9] that allows for single-shot HDR reconstruction. The MRT is based on a joint design of hardware and algorithms. HDR projections are folded into low dynamic range (LDR) measurements. This is inspired by the *Unlimited Sensing Framework* [10–14], where recovery of signals as large as $24\times$ the dynamic range of the analog-to-digital converter (ADC) has been experimentally validated (cf. [13]). Once the folded measurements are obtained (cf. Fig. 6 and Fig. 7), HDR recovery is performed using algorithmic unfolding.

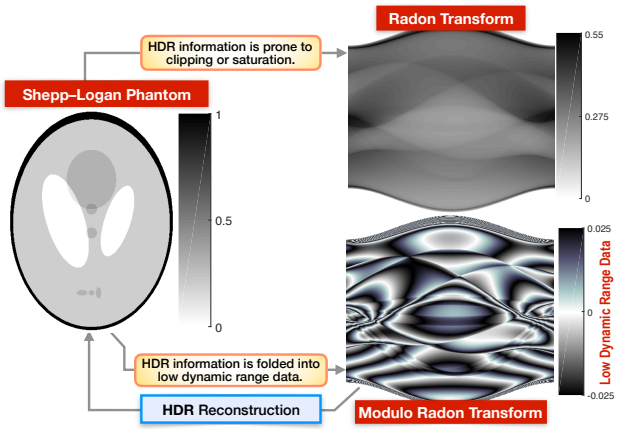

Fig. 1: Conventional Radon Transform and the corresponding Modulo Radon Transform (MRT) [1, 2] registering low dynamic range (LDR), folded projections. Algorithmic unfolding of these projections results in high dynamic range (HDR) recovery. Hardware experiments are shown in Fig. 6 and Fig. 7.

In a nutshell, the MRT is schematically explained in Fig. 1. Here, the conventional Radon Transform measurements are in the dynamic range $[0, 0.55]$. On the other hand, the MRT with modulo threshold $\lambda = 0.025$ registers much *smaller but folded*, LDR, modulo measurements. From these folded MRT measurements, HDR reconstruction is performed using the approaches in [2].

Motivation. This paper is motivated by the practical aspects of the MRT and associated experiments. In our previous work [1, 2, 9], our focus was on the inversion of the MRT as well as mathematical guarantees that back the recovery algorithms. Our recovery algorithms in [1, 2, 9] were based on higher order forward differences, which limits their practical utility in noisy scenarios and can be demanding in terms of the sampling density. This motivates the development of algorithms that (i) can work with far fewer sample sizes when compared to US-FBP method in [2], (ii) can handle noise and outliers, (iii) are agnostic to the modulo threshold λ to avoid ADC calibration and (iv) does not require the knowledge of the number of modulo folds, as is the case with the recent *Fourier–Prony* approach [13].

Contribution. In this paper, our main goal is to develop an algorithm that can handle the above-mentioned aspects (i)–(iv) simultaneously.

This work was supported by the UK Research and Innovation council's Future Leaders Fellowship program "Sensing Beyond Barriers" (MRC Fellowship award no. MR/S034897/1). Project page for (future) release of hardware design, code and data: https://bit.ly/USF-Link.

To this end, we present the **OMP-FBP method** which is based on the well-known Orthogonal Matching Pursuit (OMP) [15] algorithm. By interpreting the MRT measurements in the Fourier domain, we show that it is possible to metamorphose MRT recovery into a sparse estimation problem and this is where OMP plays a key role. In particular, realizing that modulo folds lie on a time grid allows us to build a dictionary that avoids the knowledge of modulo threshold λ. This is in contrast to unlimited sampling where λ is crucial to recovery. Furthermore, by re-interpreting Fourier domain extrapolation [13, 14] as a sparse regression problem, the OMP-FBP method avoids the knowledge of number of modulo folds. Extensive numerical experiments together with hardware validation corroborate that OMP-FBP can indeed handle far fewer samples than US-FBP [1,2,9], is robust to noise and agnostic to both modulo threshold and number of folds.

2. FORWARD MODEL AND OMP BASED RECOVERY

Forward Model. For a bivariate function $f \equiv f(\mathbf{x})$ with spatial coordinates $\mathbf{x} = (x_1, x_2) \in \mathbb{R}^2$ and threshold $\lambda > 0$, we define the *Modulo Radon Transform* (MRT) [1,2] $\mathscr{R}^\lambda f : \mathbb{S}^1 \times \mathbb{R} \longrightarrow [-\lambda, \lambda]$ of f as

$$\mathscr{R}^\lambda f(\boldsymbol{\theta}, t) = \mathscr{M}_\lambda(\mathcal{R}f(\boldsymbol{\theta}, t)),$$

where $\mathscr{M}_\lambda$ denotes the *centered* 2λ-modulo operation

$$\mathscr{M}_\lambda(t) = t - 2\lambda\Big\lfloor \frac{t+\lambda}{2\lambda} \Big\rfloor \quad \text{for } t \in \mathbb{R}$$

and $\mathcal{R}f : \mathbb{S}^1 \times \mathbb{R} \longrightarrow \mathbb{R}$ is the classical Radon Transform given by

$$\mathcal{R}f(\boldsymbol{\theta}, t) = \int_{\langle \mathbf{x}, \boldsymbol{\theta} \rangle = t} f(\mathbf{x})\, \mathrm{d}\mathbf{x}.$$

As $\boldsymbol{\theta} \in \mathbb{S}^1$ can be written as $\boldsymbol{\theta} = (\cos(\theta), \sin(\theta))$ with $\theta \in [0, 2\pi)$, we use the notations $\mathcal{R}_\theta f = \mathcal{R}f(\boldsymbol{\theta}, \cdot)$ and $\mathscr{R}^\lambda_\theta f = \mathscr{R}^\lambda f(\boldsymbol{\theta}, \cdot)$. We have proven in [2] that any band-limited function $f \in \mathrm{L}^1(\mathbb{R}^2)$ with bandwidth $\Omega > 0$ is uniquely determined by its semi-discrete MRT samples $\{\mathscr{R}^\lambda_\theta f(k\mathrm{T}) \mid \theta \in [0, \pi),\ k \in \mathbb{Z}\}$ if the sampling rate $\mathrm{T} > 0$ satisfies the oversampling condition $\mathrm{T} < \frac{\pi}{\Omega}$. To deal with not band-limited functions, we use the following sampling architecture:

(i) Pre-filter $\mathcal{R}_\theta f$ with Φ_Ω satisfying $\mathcal{F}\Phi_\Omega(\omega) = \mathbb{1}_{[-\Omega,\Omega]}(\omega)$ yielding the band-limited Radon projection $p_\theta = \mathcal{R}_\theta f * \Phi_\Omega$.
(ii) Fold p_θ into $[-\lambda, \lambda]$ giving the MRT projection $p^\lambda_\theta = \mathscr{M}_\lambda(p_\theta)$.
(iii) Sample p^λ_θ with rate T yielding $y^\lambda_\theta[k] = p^\lambda_\theta(k\mathrm{T})$ for $k \in \mathbb{Z}$.

Moreover, in practice only finitely many samples can be taken and, here, we now consider the problem of recovering $f \in \mathrm{L}^1(\mathbb{R}^2)$ with support in $B_1(0) \subset \mathbb{R}^2$, i.e., $f(\mathbf{x}) = 0$ for $\|\mathbf{x}\|_2 > 1$, from finitely many MRT projections

$$\{p^\lambda_{\theta_m}(t_k) \;\big|\; -K \le k \le K,\ 0 \le m \le M-1\}$$

in parallel beam geometry with $t_k = k\,\mathrm{T}$ and $\theta_m = m\,\frac{\pi}{M}$.

Recovery Strategy. As in [1,2,9] we follow a sequential reconstruction approach explained by the flow diagram

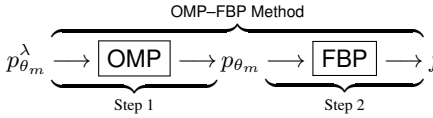

► **First Step.** Our goal here is to recover p_θ from p^λ_θ for each angle $\theta \in \{\theta_m\}_{m=0}^{M-1}$. To this end, we use Fourier series approximation, $p_\theta(t) \approx \sum_{|n| \leqslant N_\Omega} \widehat{p}_n\, \mathrm{e}^{\mathrm{i}\omega_0 n t}$ with $\omega_0 = \frac{2\pi}{\tau}$, where $\tau = (2K+1)\mathrm{T}$ and $N_\Omega = \lceil \Omega/\omega_0 \rceil$ is the effective bandwidth. Our hardware experiments in Section 3 show that this assumption is reasonable in practice. For simplicity, let us write $p_\theta[k] = p_\theta((k-K)\mathrm{T})$ and $p^\lambda_\theta[k] = p^\lambda_\theta((k-K)\mathrm{T})$ for $k \in [0, 2K]$. The modulo decomposition property [11] allows us to relate the folded samples in terms of the original samples via $p_\theta[k] = p^\lambda_\theta[k] + s^\lambda_\theta[k]$, where $s^\lambda_\theta[k] \in 2\lambda\mathbb{Z}$ is the residue function. Let Δ denote the first-difference operator and set $\underline{p}_\theta = \Delta p_\theta$. We have $\underline{p}_\theta = \underline{p}^\lambda_\theta + \underline{s}^\lambda_\theta$ revealing the sparse signal

$$\underline{s}^\lambda_\theta[k] = \sum\nolimits_{l=0}^{L_\lambda - 1} c_l\, \delta(k\mathrm{T} - t_l), \quad t_l \in (\mathrm{T}\mathbb{Z}) \cap [0, \tau)$$

where L_λ is the sparsity level depending on the number of folds induced by $\mathscr{M}_\lambda$ and $\{c_l, t_l\}_{l=0}^{L_\lambda-1}$ are the unknown parameters of the resulting sparse object. In our recent work [13], we have shown that $\underline{s}^\lambda_\theta[k]$ can be isolated in the Fourier domain. To see this in action, let us begin by denoting the Discrete Fourier Transform (DFT) of $\underline{p}_\theta[k]$ by $\widehat{\underline{p}}_\theta[n] = \sum_{k=0}^{2K-1} \underline{p}_\theta[k]\, \mathrm{e}^{-\mathrm{i}\underline{\omega}_0 nk}$, where $\underline{\omega}_0 = \frac{\pi}{K}$. Due to the band-limited approximation of p_θ by N_Ω harmonics we have

$$\widehat{\underline{p}}^\lambda_\theta[n] = \begin{cases} \widehat{\underline{p}}_\theta[n] - \widehat{\underline{s}}^\lambda_\theta[n] & n \in \mathbb{E}_{N_\Omega, 2K} \\ -\widehat{\underline{s}}^\lambda_\theta[n] & n \notin \mathbb{E}_{N_\Omega, 2K} \end{cases}$$

where $\mathbb{E}_{N_\Omega, P} = [0, N_\Omega] \cup [P - N_\Omega, P - 1]$. Hence, $\widehat{\underline{s}}^\lambda_\theta[n]$ is accessible at the Fourier frequencies $n \in [0, 2K-1] \setminus \mathbb{E}_{N_\Omega, 2K}$. Due to the explicit relation, $\widehat{\underline{s}}^\lambda_\theta[n] = \sum_{l=0}^{L_\lambda-1} c_l \exp\left(-\mathrm{i}\frac{\underline{\omega}_0 n}{\mathrm{T}} t_l\right)$ with $t_l \in (\mathrm{T}\mathbb{Z}) \cap [0, \tau)$, we can determine the $2L_\lambda$ unknowns by solving

$$\text{minimize } \|\mathbf{c}\|_0 \quad \text{such that} \quad \mathbf{V}\mathbf{c} = \mathbf{s}, \tag{1}$$

where $\mathbf{V}$ is a Vandermonde dictionary with $L = 2K+1$ columns and entries $[\mathbf{V}]_{n,l} = \exp(-\mathrm{i}\underline{\omega}_0 n l)$, $l = 0, \ldots, L-1$, $\mathbf{c} \in \mathbb{C}^L$ is the unknown sparse vector with L_λ non-zero entries, and $\mathbf{s}$ is the vector of measurements $[\mathbf{s}]_n = -\widehat{\underline{p}}^\lambda_\theta[n]$, $n \notin \mathbb{E}_{N_\Omega, 2K}$. To this end, we apply the following variant of OMP [15]:

$$\begin{cases} j_{i+1} = \underset{0 \le j \le L-1}{\arg\max} \Big| \big[\mathbf{V}^*\big(\mathbf{s} - \mathbf{V}\mathbf{c}^i\big)\big]_j \Big|, \\ \mathcal{S}^{i+1} = \mathcal{S}^i \cup \{j_{i+1}\}, \\ \mathbf{c}^{i+1} = \underset{\mathbf{c} \in \mathbb{C}^L}{\arg\min} \Big\{ \|\mathbf{s} - \mathbf{V}\mathbf{c}\|_2,\ \mathrm{supp}(\mathbf{c}) \subset \mathcal{S}^{i+1} \Big\} \end{cases} \tag{2}$$

with $\mathcal{S}^0 = \emptyset$, $\mathbf{c}^0 = 0$ and stopping criterion $\|\mathbf{V}^*(\mathbf{s} - \mathbf{V}\mathbf{c}^i)\|_\infty < \varepsilon$.

In terms of the recovery procedure, the solution to (1) provides estimates for $\{c_l, t_l\}_{l=0}^{L_\lambda-1}$. Given these estimates and $\widehat{\underline{p}}^\lambda_\theta[n]$, we can obtain $\widehat{\underline{p}}_\theta[n] = \widehat{\underline{p}}^\lambda_\theta[n] + \widehat{\underline{s}}^\lambda_\theta[n]$. There on, inverting the DFT results in $\underline{p}_\theta[k]$ and, finally, its anti-difference allows for estimation of $p_\theta[k]$.

Algorithm 1 OMP-FBP Method

Input: MRT samples $p^\lambda_\theta[k] = p^\lambda_\theta((k-K)\mathrm{T})$ for $k \in [0, 2K]$ and $\theta \in \{\theta_m\}_{m=0}^{M-1}$, bandwidth $\Omega > 0$, OMP threshold $\varepsilon > 0$

1: **for** $\theta \in \{\theta_m\}_{m=0}^{M-1}$ **do**
2: Set $\underline{p}^\lambda_\theta[n] = \Delta p^\lambda_\theta[n]$ and compute $\widehat{\underline{p}}^\lambda_\theta[n]$, $n \in [0, 2K-1]$.
3: Estimate $\{c_l, t_l\}_{l=0}^{L_\lambda-1}$ by solving (1) with OMP (2).
4: Compute $\widehat{\underline{s}}^\lambda_\theta[n] = \sum_{l=0}^{L_\lambda-1} c_l \exp\left(-\mathrm{i}\frac{\underline{\omega}_0 n}{\mathrm{T}} t_l\right)$.
5: Set $\widehat{\underline{p}}_\theta[n] = \widehat{\underline{p}}^\lambda_\theta[n] + \widehat{\underline{s}}^\lambda_\theta[n]$ and compute $\underline{p}_\theta[n]$.
6: Estimate $p_\theta[k]$, $k \in [0, 2K]$, by anti-difference.
7: **end for**

Output: OMP-FBP reconstruction $f_\Omega = \frac{1}{2}\mathcal{R}^\#_D(F_\Omega *_D p_\theta)$

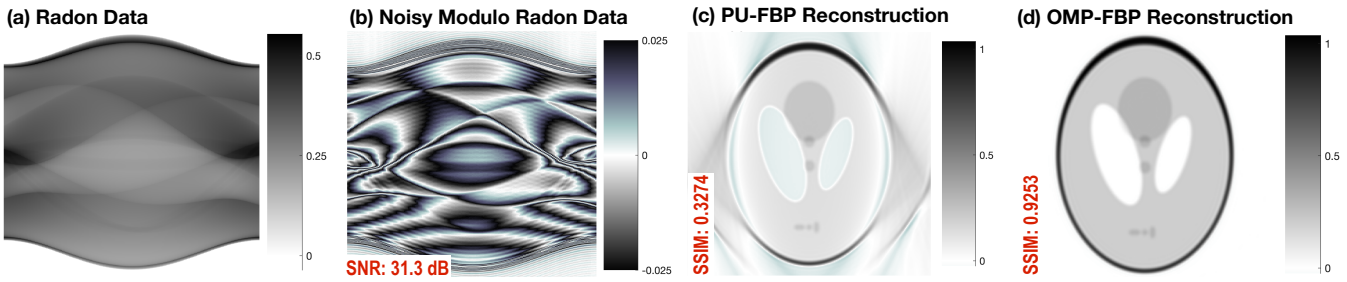

Fig. 2: Demonstration of OMP-FBP reconstruction for the Shepp-Logan phantom. (a) Radon data. (b) Noisy Modulo Radon data with $\lambda = 0.025$ and $\nu = 0.025 \cdot \lambda$. (c) PU-FBP on noisy Modulo Radon data in (b). (f) OMP-FBP on noisy Modulo Radon data in (b).

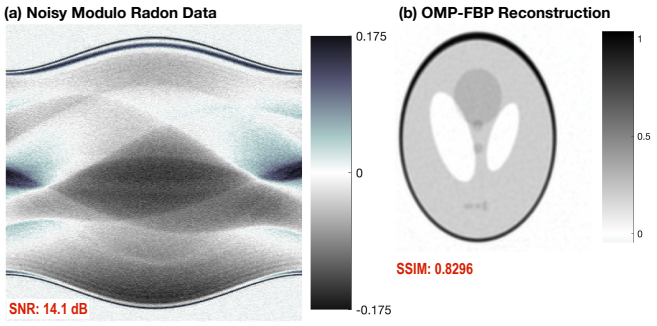

Fig. 3: OMP-FBP reconstruction from Modulo Radon data of the Shepp-Logan phantom with Gaussian and uniform noise. (a) Noisy Modulo Radon data with $\lambda = 0.175$, $\sigma = 0.025 \cdot \overline{p}_\theta$ and $\nu = 0.1 \cdot \lambda$. (b) OMP-FBP on (a).

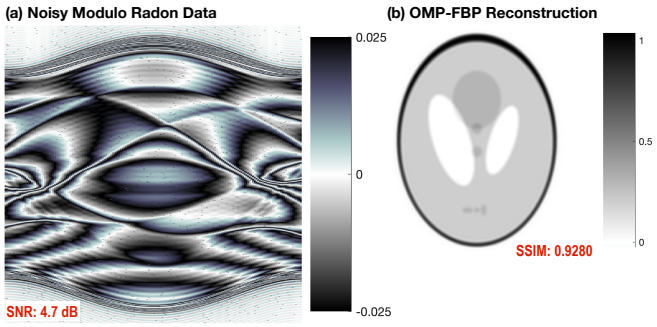

Fig. 4: OMP-FBP reconstruction from noise Modulo Radon data of the Shepp-Logan phantom with sparse outliers. (a) Noisy Modulo Radon data with $\lambda = 0.025$ and shot noise in $[-0.2, 0.2]$. (b) OMP-FBP on data in (a).

Let us stress that this approach neither uses the modulo threshold λ nor the number of folds N_λ. In particular, the application of OMP makes our recovery scheme agnostic to *both* λ and N_λ. The latter is particularly advantageous as it makes our approach data-driven in contrast to [13] which assumes the knowledge of N_λ.

► **Second Step.** Next, we reconstruct f from the recovered Radon projections $\{p_{\theta_m}(t_k) \mid -K \leq k \leq K,\ 0 \leq m \leq M-1\}$ by applying the approximate filtered back projection (FBP) formula

$$f_\Omega = \frac{1}{2}\mathcal{R}^\#(F_\Omega * p_\theta), \tag{3}$$

where F_Ω is a reconstruction filter satisfying $\mathcal{F}F_\Omega(S) = |S|\, W(\frac{S}{\Omega})$ with an even window $W \in \mathrm{L}^\infty(\mathbb{R})$ supported in $[-1, 1]$ and where $\mathcal{R}^\#$ denotes the back projection operator

$$\mathcal{R}^\# g(\mathbf{x}) = \frac{1}{2\pi}\int_{\mathbb{S}^1} g(\boldsymbol{\theta}, \mathbf{x}^\top \boldsymbol{\theta})\, \mathrm{d}\boldsymbol{\theta}.$$

As Φ_Ω and F_Ω have the same bandwidth, (3) can be rewritten as

$$f_\Omega = \frac{1}{2}\mathcal{R}^\#(F_\Omega * \mathcal{R}_\theta f)$$

and we refer to [16–18] for a discussion of reconstruction error. Our recovery scheme is summarized in Algorithm 1, where formula (3) is discretized using a standard approach, $f_{\mathrm{FBP}} = \frac{1}{2}\mathcal{R}_D^\#(F_\Omega *_D p_\theta)$. According to [19], the optimal sampling conditions for fixed bandwidth $\Omega > 0$ are given by $\mathrm{T} \leq \frac{\pi}{\Omega}$, $K \geq \frac{1}{\mathrm{T}}$ and $M \geq \Omega$.

3. NUMERICAL AND HARDWARE EXPERIMENTS

We now present numerical and hardware experiments to demonstrate the effectivity of our approach for both simulated and real data. We use the Shepp-Logan phantom [20] and the open source walnut dataset [21] that includes realistic uncertainties arising from the tomography hardware. For comparison, we also apply US-FBP [2] based on Unlimited Sampling Algorithm (USAlg) [11] and PU-FBP based on Phase Unwrapping (PU) in the first Step of our approach.

Numerical Experiments. In a first set of numerical experiments we use the OMP-FBP framework to recover the Shepp-Logan phantom on a grid of 256×256 pixels from noisy Modulo Radon Projections $\{\tilde{p}^\lambda_{\theta_m}(k\mathrm{T}) \mid -K \leq k \leq K,\ 0 \leq m \leq M-1\}$, where we always use the optimal parameter choices $\mathrm{T} = 1/K$, $\Omega = M$ and the cosine reconstruction filter given by $\mathcal{F}F_\Omega(\omega) = |\omega|\, \cos(\frac{\pi\omega}{2\Omega})\, \mathbb{1}_{[-\Omega,\Omega]}(\omega)$. The results for $\lambda = 0.025$ are summarized in Fig. 2, where we use the parameters $K = 698$, $M = 180$ and uniform noise with noise level $\nu = 0.025 \cdot \lambda$ on the modulo samples, i.e., $\|\tilde{p}^\lambda_\theta - p^\lambda_\theta\|_\infty \leq \nu$, leading to an SNR of 31.3 dB. This choice violates the recovery conditions for USAlg, namely, $\mathrm{T}_{\mathrm{US}} \leq \frac{1}{2\Omega e}$, and hence, US-FBP recovery fails. Also PU is not applicable and PU-FBP fails as well. In contrast to this, OMP-FBP successfully recovers with structural similarity index measure [22] $\mathsf{SSIM} = 0.9253$ at the same quality as FBP reconstruction from clear Radon data, where $\mathsf{SSIM} = 0.9285$.

In Fig. 3 we use the parameters $K = 574$, $M = 180$ and consider a combination of Gaussian noise before and uniform noise after modulo with threshold $\lambda = 0.175$. We added white Gaussian noise with variance σ^2 to the Radon projections p_θ, where $\sigma = 0.025 \cdot \overline{p}_\theta$ depends on the arithmetic mean $\overline{p}_\theta$ of p_θ. Moreover, we added uniform noise with noise level $\nu = 0.1 \cdot \lambda$ to the modulo projections, yielding the noisy projections $\tilde{p}^\lambda_\theta$ with an SNR of 14.1 dB. We observe that OMP-FBP is able to reconstruct the phantom from this noisy data with $\mathsf{SSIM} = 0.8296$, which is comparable to the FBP reconstruction from the noisy Radon data, where $\mathsf{SSIM} = 0.9069$.

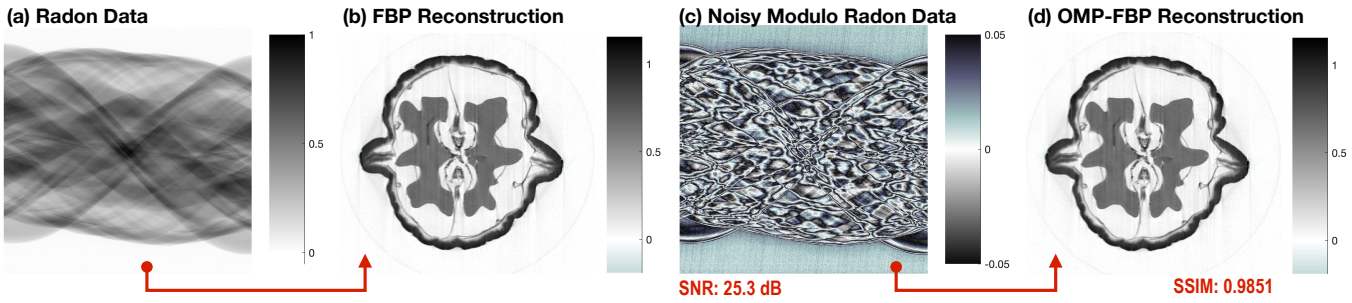

Fig. 5: Demonstration of OMP-FBP reconstruction for the walnut dataset. (a) Normalized Radon data. (b) FBP on Radon data in (a) serving as ground truth. (c) Noisy Modulo Radon data with $\lambda = 0.05$ and $\nu = 0.05 \cdot \lambda$. (d) OMP-FBP on noisy Modulo Radon data in (c).

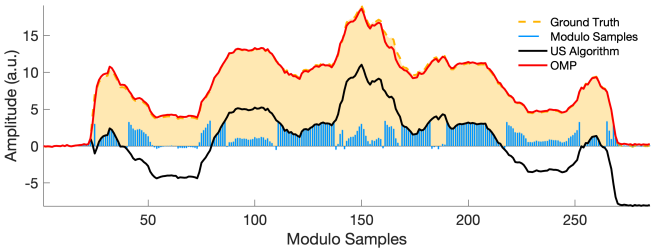

Fig. 6: Hardware validation of our OMP-FBP approach on the walnut dataset with our prototype modulo sampling hardware and subsampling factor 2.33.

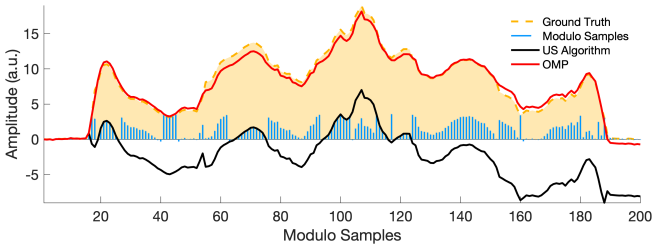

Fig. 7: Hardware validation of our OMP-FBP approach on the walnut dataset with our prototype modulo sampling hardware and subsampling factor 3.33.

To simulate the observation that real hardware modulo samples can be contaminated with sparse outliers, we consider the case of shot noise in Fig. 4. For each angle θ we added random values in the range $[-0.2, 0.2]$ at up to 20 positions to the Modulo Radon Projections p_θ^λ with threshold $\lambda = 0.025$ and parameters $K = 821$, $M = 180$, i.e., $\|\tilde{p}_\theta^\lambda - p_\theta^\lambda\|_\infty \leq 0.2$ and $\|\tilde{p}_\theta^\lambda - p_\theta^\lambda\|_0 \leq 20$, leading to an SNR of 4.7 dB. While US-FBP and PU-FBP fail, OMP-FBP successfully recovers with $\mathsf{SSIM} = 0.9280$ at the same quality as the FBP reconstruction from clear Radon data, where $\mathsf{SSIM} = 0.9285$.

In a second set of experiments, we consider the walnut dataset from [21], which is transformed to parallel beam geometry with $M = 600$ and $K = 1128$ corresponding to $\mathrm{T} = 1/1128$. Moreover, the Radon data is normalized to the dynamical range $[0, 1]$ so that $\|\mathcal{R}f\|_\infty = 1$. Its simulated Modulo Radon Projections are displayed in Fig. 5(c) for $\lambda = 0.025$, where we added uniform noise with noise level $\nu = 0.05 \cdot \lambda$ to the modulo samples to account for quantization errors, i.e., $\|\tilde{p}_\theta^\lambda - p_\theta^\lambda\|_\infty \leq \nu$, leading to an SNR of 25.3 dB. The reconstruction with our proposed OMP-FBP method is shown in Fig. 5(d), where we again use $\Omega = M = 600$ and the cosine reconstruction filter. We observe that our algorithm yields a reconstruction of the walnut that is again visually indistinguishable from the FBP reconstruction from conventional Radon data, cf. Fig. 5(b), while compressing the dynamic range by about 10 times.

Hardware Experiments. We validate the effectivity of our OMP based approach on real data which is prone to system noise [11] and outliers [14]. To do so, we consider MRT samples acquired by our custom designed modulo ADC [13]. In particular, Radon Transform measurements based on the *walnut dataset* [21] are re-digitized using our modulo ADC. For further details on the acquisition protocol, we refer to Section 4.2 in [2]. We consider MRT samples along two different angles θ. As mentioned in our work, the use of OMP based approach allows for recovery at reduced sampling rates. MRT data acquired using $\mathrm{T} = 75$ μsec. (sampling period) and $N = 665$ samples with $\Omega_{\mathsf{Hz}} \approx 1000$ Hz allows for recovery with $\lambda = 2.01$ when using the US-FBP method [2]. Here, in Fig. 6, we consider $N = 285$ samples at $\mathrm{T}_{\mathsf{OMP}} = 175\mu$sec., which is a factor $2.33\times$ reduction. This violates the recovery condition for the USAlg [11], namely, $\mathrm{T}_{\mathsf{US}} \leq 1/2\Omega e$ and hence, USAlg based recovery fails. That said, the OMP based approach recovers the HDR signal with $\mathsf{MSE} = 9.79 \times 10^{-2}$ and is agnostic to both λ and N_λ.

In Fig. 7, we consider a more aggressive reduction in sampling density, that is $N = 200$ MRT samples with $\mathrm{T}_{\mathsf{OMP}} = 250\mu$sec. which amounts to a factor $3.33\times$ reduction in comparison to [2]. Not surprisingly, the US-FBP method is unable to recover while OMP based approach offers a graceful recovery with $\mathsf{MSE} = 3.88 \times 10^{-1}$.

4. CONCLUSION

The Modulo Radon Transform (MRT) has been recently introduced to offer an alternative approach towards high dynamic range (HDR) tomography. Instead of combining multiple Radon Transform projections at different exposures, as is the case with conventional HDR photography, the MRT achieves this goal in a single shot approach. In the case of MRT, arbitrarily large Radon projections are folded into the dynamic range of the analog-to-digital converter and there on, HDR recovery boils down to the inverse problem of "unfolding" the folded projections. To this end, this paper introduces a Fourier domain recovery termed as the OMP-FBP approach. This method leverages sparsity and is based on the orthogonal matching pursuit (OMP) algorithm. Both computer and hardware experiments, based on our custom designed modulo-ADC, show the benefits of our approach. In particular, the OMP-FBP method offers recovery at lower sampling rates and is robust to noise and outliers. At the same time, the OMP-FBP approach is agnostic to the modulo threshold and the number of modulo folds. Our current work is grounded in experiments with emphasis on hardware measurements to develop a sense of realistic performance. Future work includes developing concrete recovery guarantees and noise performance analysis.

5. REFERENCES

[1] A. Bhandari, M. Beckmann, and F. Krahmer, "The Modulo Radon Transform and its inversion," in *European Sig. Proc. Conf. (EUSIPCO)*, Oct. 2020, pp. 770–774.

[2] M. Beckmann, F. Krahmer, and A. Bhandari, "The modulo Radon transform: Theory, algorithms and applications," *(in press) SIAM Journal of Imaging Sciences*, Nov. 2021.

[3] P. Chen, Y. Han, and J. Pan, "High-dynamic-range CT reconstruction based on varying tube-voltage imaging," *PLOS ONE*, vol. 10, no. 11, p. e0141789, Nov. 2015.

[4] J. T. Weiss, K. S. Shanks, H. T. Philipp, J. Becker, D. Chamberlain, P. Purohit, M. W. Tate, and S. M. Gruner, "High dynamic range X-Ray detector pixel architectures utilizing charge removal," *IEEE Trans. Nucl. Sci.*, vol. 64, no. 4, pp. 1101–1107, Apr. 2017.

[5] M. A. Haidekker, L. D. Morrison, A. Sharma, and E. Burke, "Enhanced dynamic range X-ray imaging," *Computers in Biology and Medicine*, vol. 82, pp. 40–48, Mar. 2017.

[6] Y. Li, Y. Han, and P. Chen, "X-ray energy self-adaption high dynamic range (HDR) imaging based on linear constraints with variable energy," *IEEE Photon. J.*, vol. 10, no. 2, pp. 1–14, Apr. 2018.

[7] A. Bhandari, A. Kadambi, and R. Raskar, *Computational Imaging*, 1st ed. MIT Press, Jun. 2022,
Open Access URL: https://imagingtext.github.io/.

[8] P. E. Debevec and J. Malik, "Recovering high dynamic range radiance maps from photographs," in *ACM Transactions on Graphics*. ACM Press, 1997.

[9] M. Beckmann, F. Krahmer, and A. Bhandari, "HDR tomography via modulo Radon transform," in *IEEE Intl. Conf. on Image Processing (ICIP)*, Oct. 2020, pp. 3025–3029.

[10] A. Bhandari, F. Krahmer, and R. Raskar, "On unlimited sampling," in *Intl. Conf. on Sampling Theory and Applications (SampTA)*, Jul. 2017.

[11] ——, "On unlimited sampling and reconstruction," *IEEE Trans. Sig. Proc.*, vol. 69, pp. 3827–3839, Dec. 2020.

[12] A. Bhandari and F. Krahmer, "HDR imaging from quantization noise," in *IEEE Intl. Conf. on Image Processing (ICIP)*, Oct. 2020, pp. 101–105.

[13] A. Bhandari, F. Krahmer, and T. Poskitt, "Unlimited sampling from theory to practice: Fourier-Prony recovery and prototype ADC," *IEEE Trans. Sig. Proc.*, Sep. 2021.

[14] A. Bhandari, "Unlimited sampling with sparse outliers: Experiments with impulsive and jump or reset noise," in *IEEE Intl. Conf. on Acoustics, Speech and Sig. Proc. (ICASSP) (to appear)*, 2022.

[15] S. Foucart and H. Rauhut, *A Mathematical Introduction to Compressive Sensing*, ser. Applied and Numerical Harmonic Analysis. Birkhäuser, 2013.

[16] M. Beckmann and A. Iske, "Error estimates and convergence rates for filtered back projection," *Mathematics of Computation*, vol. 88, no. 316, pp. 801–835, 2019.

[17] ——, "Saturation rates of filtered back projection approximations," *Calcolo*, vol. 57, no. 1, p. 12, 2020.

[18] M. Beckmann, P. Maass, and J. Nickel, "Error analysis for filtered back projection reconstructions in Besov spaces," *Inverse Problems*, vol. 37, no. 1, p. 014002, 2021.

[19] F. Natterer and F. Wübbeling, *Mathematical methods in image reconstruction*, ser. SIAM Monographs on Mathematical Modeling and Computation. SIAM, 2001.

[20] L. A. Shepp and B. F. Logan, "The Fourier reconstruction of a head section," *IEEE Trans. Nucl. Sci.*, vol. 21, no. 3, pp. 21–43, 1974.

[21] K. Hämäläinen, L. Harhanen, A. Kallonen, A. Kujanpää, E. Niemi, and S. Siltanen, "Tomographic X-ray data of a walnut," Zenodo (URL: https://zenodo.org/record/1254206), 2015.

[22] Z. Wang, A. Bovik, H. Sheikh, and E. Simoncelli, "Image quality assessment: from error visibility to structural similarity," *IEEE Trans. Image Proc.*, vol. 13, no. 4, pp. 600–612, 2004.